

Figure 4 Isolation

4. EXPERIMENTAL RESULTS

The proof of concept follows a design methodology, demonstrated by using a commercial GaAs FET, Avago Technologies, ATF-34143. The FETs were biased with a drain source voltage of 4 V and a drain current of 15 mA. A demonstration of the circulator uses a single stage FET implementation in both the distributed balun and single distributed combiner. The series inductors and series capacitors were implemented using microstrip lines and surface mount components respectively. S-parameter plots of the measured results are shown in Figures 3 and 4 for the circulator (using Agilent E5071B ENA network analyzer). The return losses of the three ports are greater than 10 dB, whereas the insertion losses S_{21} and S_{32} are around $0 \text{ dB} \pm 1.5 \text{ dB}$. Between the frequency ranges of 0.8–2.2 GHz, the minimum isolation between Ports 1 and 3 is around 20 dB due to the self-equalization technique, with greater than 20 dB between the other ports due to the FET unilateral characteristic.

5. CONCLUSIONS

A simple self-equalization technique for a distributed quasi-circulator has been proposed with experimental results verifying its wideband operation. Future portable handsets such as software defined radio will have potential use of this topology because it provides wideband frequency operation invisible to multiple access methods. This concept is suitable for circuit miniaturization as well as in mobile handsets.

ACKNOWLEDGMENTS

The authors thank the City University of Hong Kong (Research Project 7002242) for the financial support of the work carried out here.

REFERENCES

1. J.B. Beyer, S.N. Prasad, R.C. Becker, J.E. Nordman, and G.K. Hohenwarter, MESFET distributed amplifier design guidelines, *IEEE Trans Microwave Theory Tech* 32 (1984), 268–275.
2. O.S.A. Tang and C.S. Aitchison, A very wide-band microwave MESFET mixer using the distributed mixing principle, *IEEE Trans Microwave Theory Tech* 33 (1985), 1470–1478.
3. O.P. Leisten, R.J. Collier, and R.N. Bates, Distributed amplifiers as duplexer/low crosstalk bidirectional elements in S-band, *Electron Lett* 24 (1988), 264–265.
4. D. Kother, B. Hopf, T. Sporkmann, I. Wolff, and S. Kołowski, New types of MMIC circulators, *IEEE MTT-S Int Microwave Symp Dig*, Orlando, FL (1995), 877–880.
5. A.H. Barea and I.D. Robertson, Monolithic MESFET distributed baluns

based on the distributed amplifier gate-line termination technique, *IEEE Trans Microwave Theory Tech* 45 (1997), 188–195.

6. R. Majidi-Ahy, C. Nishimoto, J. Russell, W. Ou, S. Bandy, G. Zdziusik, C. Shih, Y.C. Pao, and C. Yuen, 4–40 GHz MMIC distributed active combiner with 3 dB gain, *Electron Lett* 28 (1992), 739–741.
7. S.N. Prasad, J.B. Beyer, and I.S. Chang, Power-bandwidth considerations in the design of MESFET distributed amplifiers, *IEEE Trans Microwave Theory Tech* 36 (1988), 1117–1123.

© 2008 Wiley Periodicals, Inc.

VERY-SMALL-SIZE PRINTED LOOP ANTENNA FOR GSM/DCS/PCS/UMTS OPERATION IN THE MOBILE PHONE

Yun-Wen Chi and Kin-Lu Wong

Department of Electrical Engineering, National Sun Yat-Sen University, Kaohsiung 80424, Taiwan; Corresponding author: chiyw@ema.ee.nsysu.edu.tw

Received 14 May 2008

ABSTRACT: A very-small-size printed loop antenna for mobile phone application is proposed. The antenna has a loop strip of length 62 mm only, which is folded into an L-shape and occupies a small area of 96.5 mm² on the top no-ground portion of the system circuit board of the mobile phone. By incorporating a simple matching circuit formed by a chip capacitor and a chip inductor, both in series, the loop antenna can generate three resonant modes (0.25-, 0.5-, and 1.0-wavelength modes) at about 925, 1800, and 2200 MHz. The 0.25-wavelength mode forms the antenna's lower band covering GSM operation, whereas the 0.5- and 1.0-wavelength modes form the antenna's upper band covering DCS/PCS/UMTS operation. Quad-band operation is hence obtained for the printed loop antenna, although it has a very small size. Details of the proposed antenna are presented. © 2008 Wiley Periodicals, Inc. *Microwave Opt Technol Lett* 51: 184–192, 2009; Published online in Wiley InterScience (www.interscience.wiley.com). DOI 10.1002/mop.24008

Key words: mobile phone antennas; quarter-wavelength loop antennas; printed antennas; internal mobile phone antennas; multiband operation

1. INTRODUCTION

Multiband operation has recently become a demanding requirement for internal antennas to be employed in the mobile phone for WWAN (wireless wide area network) operation. Further, the occupied size of the promising multiband internal antennas inside the mobile phone is required to be as small as possible. In the recent studies [1–7], the loop antennas have been shown to be promising candidates for application in the mobile phone as internal multiband antennas with reasonable occupied size. These multiband loop antennas are generally achieved by printing the desired loop metal pattern on the system circuit board or thin dielectric substrate [1–3], forming the loop metal pattern on the surfaces of the chip base as surface-mount elements [4], or mounting the loop metal strip above the system ground plane of the mobile phone [5–7]. For these reported loop antennas, however, they are mainly operated at their 0.5-wavelength resonant mode to form the antenna's lower band to cover GSM (890–960 MHz) operation. This is a great limitation in further size reduction of the loop antenna for mobile phone application.

In this article, we demonstrate the first time the multiband printed loop antenna operated at its 0.25-wavelength resonant mode as the fundamental mode for mobile phone application. The proposed printed loop antenna has a folded loop metal strip of

length 62 mm (about 0.19 wavelength of the frequency at 900 MHz) printed on the top no-ground portion of the system circuit board. The antenna incorporates a simple series LC matching circuit, which effectively compensates for the large inductive reactance of the input impedance of the antenna's 0.25-wavelength mode and also shows constructive effects on improving the impedance matching of the antenna's 0.5- and 1.0-wavelength modes. Three resonant modes (0.25-, 0.5-, and 1.0-wavelength modes) at about 925, 1800, and 2200 MHz can hence be excited for the proposed loop antenna to cover the GSM, DCS (1710–1880 MHz), PCS (1850–1990 MHz), and UMTS (1920–2170 MHz) bands [8] for multiband operation. Note that the matching circuit applied here leads to the excitation of a much lower first resonant mode for the internal antenna in the mobile phone. This behavior is greatly different from that of the conventional matching circuits [9–13], which are mainly used for bandwidth widening of the existing resonant modes of the internal mobile phone antenna. Detailed discussions on the effects of the applied matching circuit on the proposed printed loop antenna are given in this study. Experimental results of the printed loop antenna with the matching circuit are also presented.

2. PROPOSED PRINTED LOOP ANTENNA

Figure 1(a) shows the geometry of the printed loop antenna with the series LC matching circuit, and the detailed dimensions are

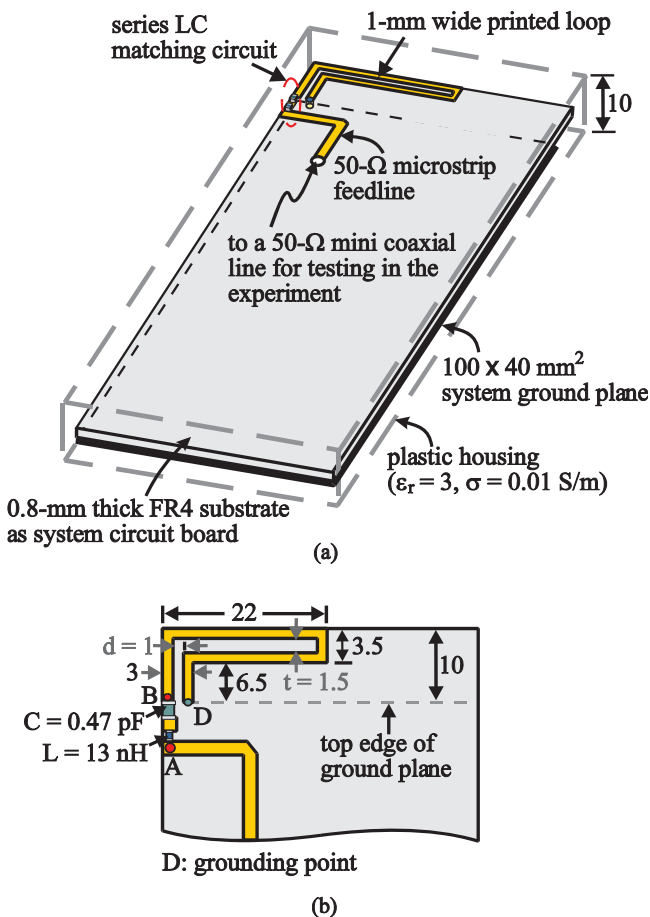


Figure 1 (a) Geometry of the printed loop antenna with the series LC matching circuit for mobile phone application. (b) Dimensions of the printed loop and the matching circuit. [Color figure can be viewed in the online issue, which is available at www.interscience.wiley.com]

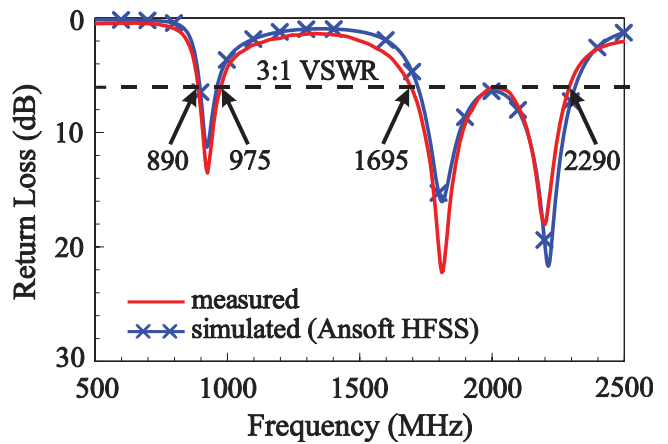


Figure 2 Measured and simulated return loss for the proposed antenna. [Color figure can be viewed in the online issue, which is available at www.interscience.wiley.com]

given in Figure 1(b). As shown in the figure, a 0.8-mm thick FR4 substrate of size $40 \times 110 \text{ mm}^2$ is used in the study as the system circuit board of the mobile phone. A system ground plane of size $40 \times 100 \text{ mm}^2$ is printed on the back side of the circuit board, leaving a no-ground portion of size $40 \times 10 \text{ mm}^2$ at the top region of the circuit board. The loop antenna is printed on the no-ground portion and consists of a 1-mm wide metal strip folded into an L-shape. One end (point D) of the folded loop strip is grounded to the top edge of the system ground plane through a via-hole in the circuit board. The other end (point B) of the folded loop strip is connected to the series LC matching circuit, which is then connected to the 50- Ω microstrip feedline printed on the front side of the circuit board for testing in the experiment. Note that there is also a plastic housing made of 1-mm thick ABS (Acrylonitrile Butadiene Styrene, relative permittivity 3.0 and conductivity 0.01 S/m) enclosing the system circuit board to simulate the practical mobile phone with a plastic housing.

The printed loop strip has a length of 62 mm only (from point B to point D), corresponding to about 0.19 wavelength of the frequency at 900 MHz. By folding the loop strip into an L-shape, it shows a lateral length of 22 mm only and occupies a small area of 96.5 mm^2 ($22 \times 3.5 \text{ mm}^2 + 3 \times 6.5 \text{ mm}^2$) on the top no-ground

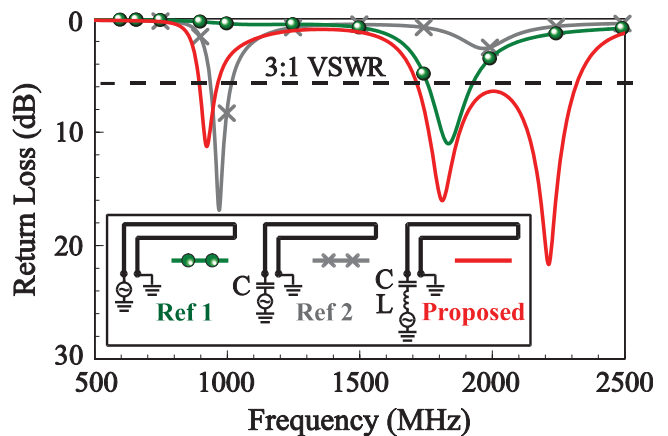
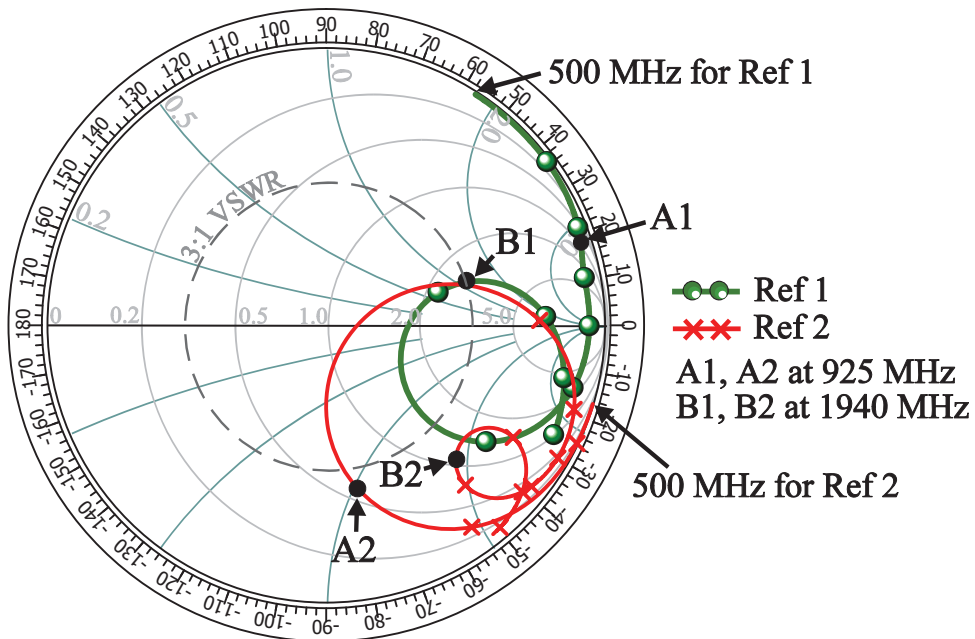


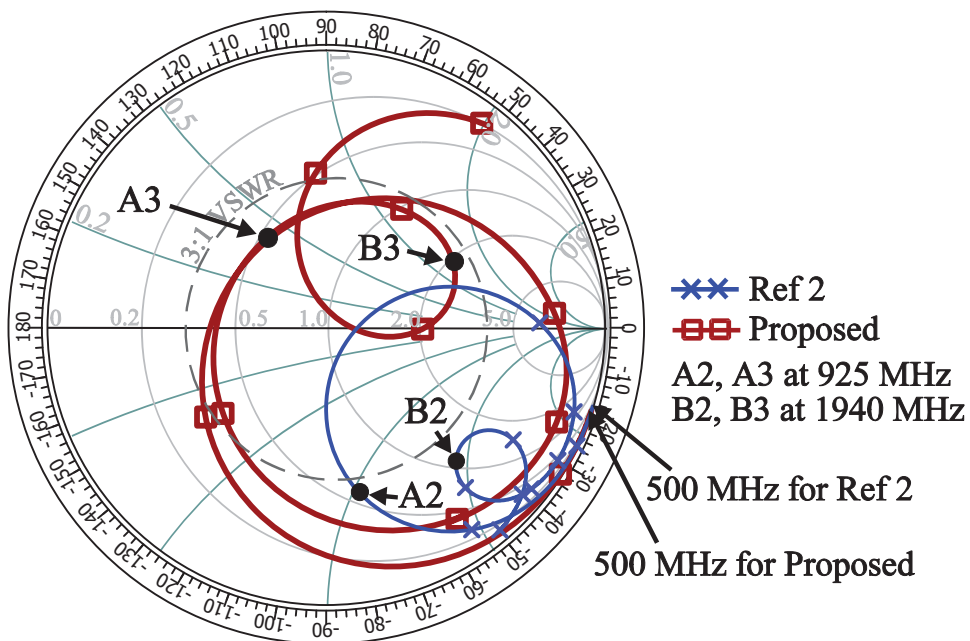
Figure 3 Comparison of the simulated return loss for the proposed antenna, the case without the matching circuit [1], and the case with the capacitor-only matching circuit [2]. [Color figure can be viewed in the online issue, which is available at www.interscience.wiley.com]

portion. With the small lateral length, which is only about half of the width of general mobile phones, the loop antenna can be placed at around one of the corners of the top no-ground portion, leaving a large unoccupied region at the top of the circuit board to accommodate the possible elements like the speaker [14, 15], the

embedded digital camera [16], etc. This feature is obtained owing to the very small size of the printed loop antenna studied here, which is an advantage over the conventional internal mobile phone antennas which usually occupy the whole top portion of the mobile phone.



(a)



(b)

**All curves: start at 500 MHz and end at 2500 MHz
Interval between two marks: 200 MHz**

Figure 4 Comparison of the simulated input impedance on the Smith chart. (a) The case without the matching circuit [1] and the case with the capacitor-only matching circuit [2]. (b) Ref. [1] and the proposed antenna. [Color figure can be viewed in the online issue, which is available at www.interscience.wiley.com]

TABLE 1 Simulated Input Impedance at the Reference Points

$f_1 = 925$ MHz		$f_2 = 1940$ MHz	
Reference point	$Z = R + jX$ (Ω)	Reference point	$Z = R + jX$ (Ω)
A1	$30 + j287$	B1	$145 + j67$
A2	$28 - j60$	B2	$75 - j105$
A3	$31 + j21$	B3	$100 + j49$

Note that when there is no matching circuit incorporated with the printed loop strip, the antenna can only generate a 0.5λ mode at about 1800 MHz, because the loop strip has a short length of 62 mm only. In this case, input impedance of the 0.25λ mode of the loop antenna is found to have a large inductive reactance, which makes the 0.25λ mode difficult to be excited with good impedance matching. By incorporating the matching circuit with a series chip capacitor C of 0.47 pF and a series chip inductor L of 13 nH [see Fig. 1(b)], the large inductive reactance of the 0.25λ mode can be compensated and good excitation of the 0.5λ and 1.0λ modes can also be obtained as well. Details on selecting the values of the

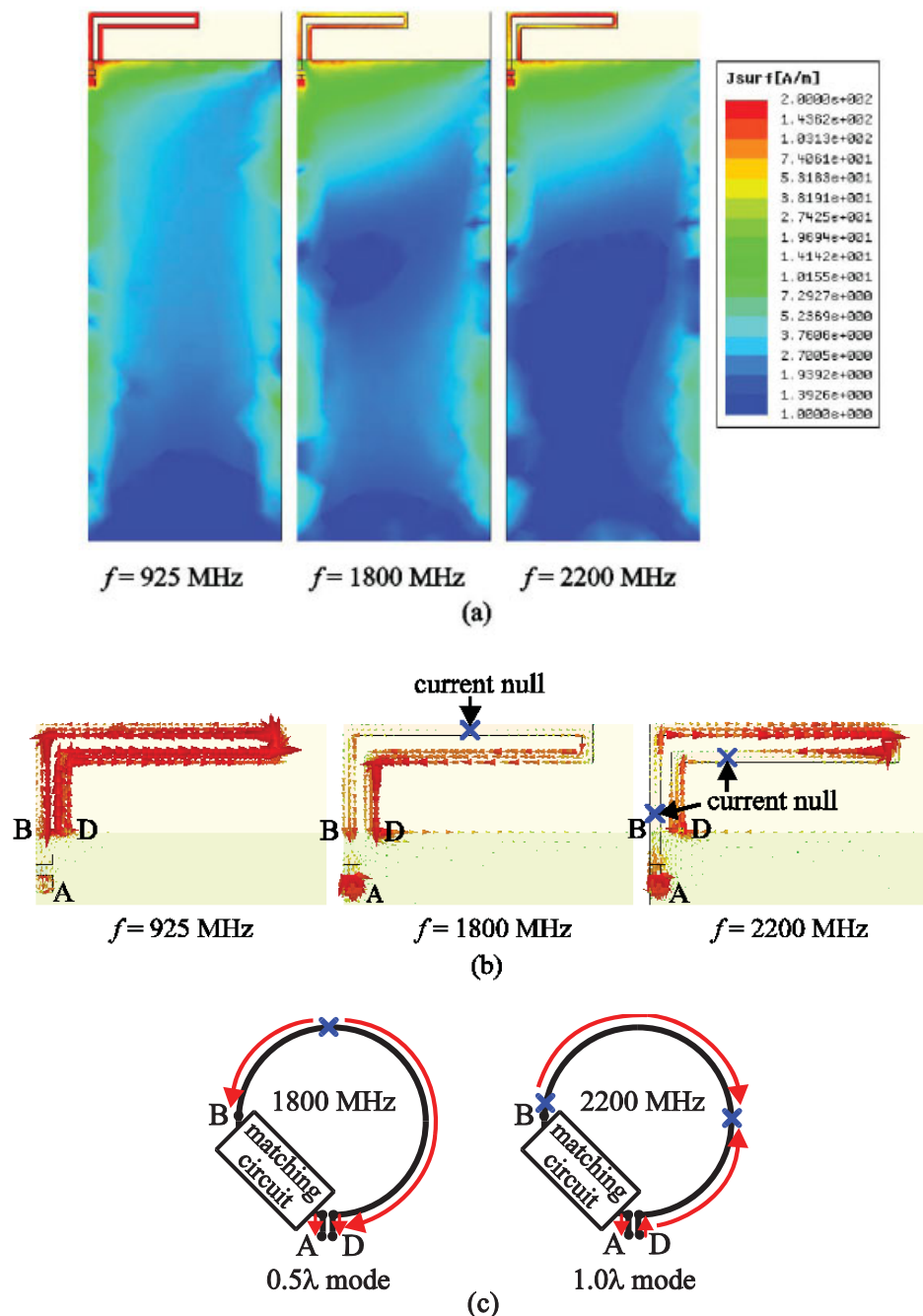


Figure 5 Simulated excited surface currents at 925, 1800, and 2200 MHz on the loop strip and the system ground plane. (a) Magnitude of the surface currents. (b) Vector surface currents on the loop strip. (c) Equivalent surface currents for the 0.5λ and 1.0λ modes of the loop antenna including the matching circuit. [Color figure can be viewed in the online issue, which is available at www.interscience.wiley.com]

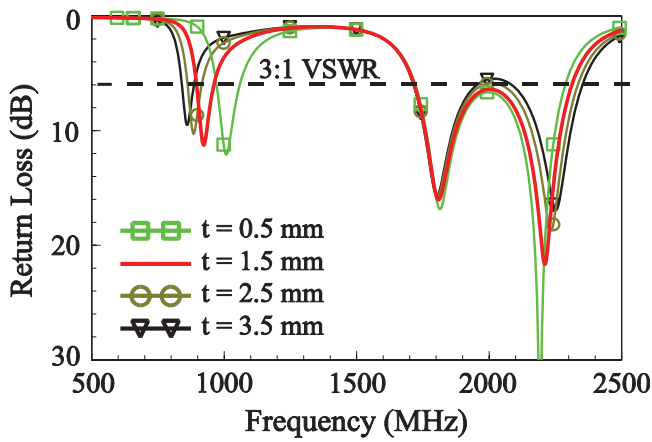


Figure 6 Simulated return loss as a function of the gap width t in the folded loop strip. Other dimensions are the same as studied in Figure 2. [Color figure can be viewed in the online issue, which is available at www.interscience.wiley.com]

series capacitor and inductor are discussed in Section 3 with the aid of Figure 4.

In the folded loop strip, there are also two parameters t and d capable of adjusting the resonant frequencies of the three excited resonant modes (0.25λ , 0.5λ , and 1.0λ modes). The parameters t and d are the gap widths in the middle part and front part of the folded loop strip, respectively. By varying t and d , the coupling between the strip sections in the middle part and front part will be varied, which can lead to some variations in the excited surface current distributions of the 0.25λ , 0.5λ , and 1.0λ modes of the loop antenna. This, in turn, will lead to some shifting in the resonant frequencies of the antenna's three excited resonant modes. Their detailed effects will be discussed in Figures 6 and 7 in the next section.

3. RESULTS AND DISCUSSION

On the basis of the design dimensions shown in Figure 1, which are the preferred dimensions in this study, the proposed antenna was constructed and tested. Figure 2 shows the measured and simulated return loss of the constructed prototype. The simulated results are obtained using Ansoft HFSS [17], and good

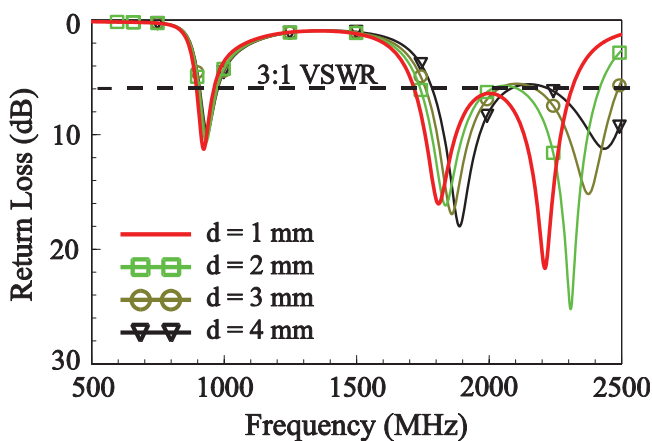


Figure 7 Simulated return loss as a function of the gap width d in the folded loop strip. Other dimensions are the same as studied in Figure 2. [Color figure can be viewed in the online issue, which is available at www.interscience.wiley.com]

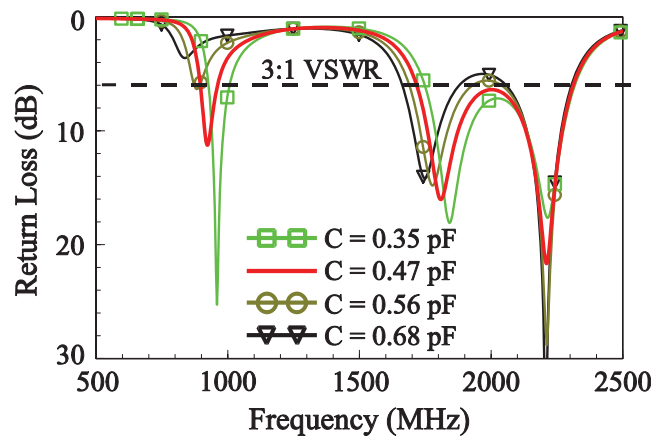


Figure 8 Simulated return loss as a function of the chip capacitor C . Other dimensions are the same as studied in Figure 2. [Color figure can be viewed in the online issue, which is available at www.interscience.wiley.com]

agreement between the measurement and simulation is seen. As discussed in Section 2, three resonant modes with good impedance matching are excited. The antenna's lower band at about 900 MHz is formed by the first resonant mode (0.25λ mode) with a bandwidth of 85 MHz (890–975 MHz), suitable for GSM operation.

The second and third resonant modes (0.5λ and 1.0λ modes) form the antenna's upper band, which shows a large bandwidth of 595 MHz (1695–2290 MHz) and covers DCS/PCS/UMTS operation. Note that the bandwidth definition used here is 3:1 VSWR, which is a general standard for practical mobile phone applications.

Figure 3 shows the comparison of the simulated return loss for the proposed antenna with the LC matching circuit (Proposed), the case without the matching circuit [1], and the case with the capacitor-only matching circuit [2]. The three cases are also shown in the inset of Figure 3. It is seen that only one resonant mode (0.5λ mode) at about 1800 MHz is excited for [1], and its operating bandwidth (3:1 VSWR) is only about 150 MHz. When the capacitor-only ($C = 0.47$ pF) matching circuit is added [2], a new resonant mode (0.25λ mode) at about 1000 MHz is excited, and

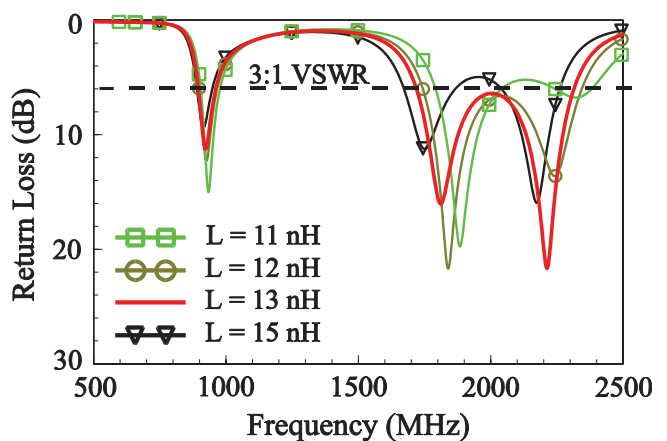


Figure 9 Simulated return loss as a function of the chip inductor L . Other dimensions are the same as studied in Figure 2. [Color figure can be viewed in the online issue, which is available at www.interscience.wiley.com]

however, the impedance matching of the 0.5λ mode at about 1800 MHz is degraded. By further adding an inductor of $L = 13$ nH for the proposed antenna, the impedance matching of the 0.5λ mode is improved, which incorporates a new excited resonant mode (1.0λ mode) to form a wide upper band for the antenna to cover DCS/PCS/UMTS operation. Also, the 0.25λ mode is shifted to be at 900 MHz to cover GSM operation.

To show more clearly the effects of adding the capacitor ($C = 0.47$ pF) and the inductor ($L = 13$ nH), a comparison of the simulated input impedance on the Smith chart for the three antennas studied in Figure 3 are also presented in Figure 4. Figure 4(a) shows the comparison of the simulated input impedance of [1] and [2], whereas Figure 4(b) shows that of [2] and proposed. All the curves start at 500 MHz and end at 2500 MHz, and the interval between two marks is 200 MHz. The frequency at reference points A_1 , A_2 , and A_3 is 925 MHz (center frequency of the GSM band), while that at reference points B_1 , B_2 , and B_3 is 1940 MHz (center frequency of DCS/PCS/UMTS bands). The input impedances at these points are listed in Table 1, with points A_1 and B_1 for [1], points A_2 and B_2 for [2], and points A_3 and B_3 for Proposed.

It is seen that point A_1 for [1] has a large inductive reactance of 287Ω , which is compensated to be $-j60 \Omega$ at point A_2 for [2] by adding a capacitor of 0.47 pF. However, in this case, the inductive reactance ($j67 \Omega$) at point B_1 becomes capacitive reactance ($-j105 \Omega$) at point B_2 for [2]. By further adding a series inductor of 13 nF, the reactance at points A_3 and B_3 for Proposed can both be decreased to achieve good impedance matching. The proper capacitance C and inductance L in this study can be easily selected by solving Eqs. (1) and (2):

$$j2\pi f_1 L - j/2\pi f_1 C \approx -j287 \Omega, \quad (1)$$

$$j2\pi f_2 L - j/2\pi f_2 C \approx 0 \Omega, \quad (2)$$

where f_1 and f_2 are the central frequencies (925 and 1940 MHz) of the desired lower and upper bands of the antenna, respectively. For L and C satisfying Eqs. (1) and (2), the large inductive reactance at point A_1 can be compensated, with small effects on the acceptable reactance level at point B_1 . Equations (1) and (2) are solved

to obtain $C = 0.464$ pF and $L = 14.5$ nH. However, for the available 0805 chip capacitor series and 0603 chip inductor series, the capacitor and inductor that we can obtain is 0.47 pF and 13 nH, respectively. With the two selected elements in the LC matching circuit, the impedance matching at points A_3 and B_3 for the proposed antenna is compensated to acceptable level as shown in Figure 4(b). Further, it is found that an additional mode (1.0λ mode) at about 2200 MHz is also generated owing to the added matching circuit. The 1.0λ mode and the 0.5λ mode are formed into a wide upper band for the proposed antenna to cover GSM/DCS/UMTS operation.

To study the excited three resonant modes (0.25λ , 0.5λ , and 1.0λ modes) at 925, 1800, and 2200 MHz, Figure 5 shows their simulated excited surface currents on the loop strip and the system ground plane. In Figure 5(a), it is seen that the surface currents on the ground plane at 925 MHz is stronger than those at 1800 and 2200 MHz. This behavior is similar to the conventional planar inverted-F antenna (PIFA) whose first resonant mode is also the 0.25λ mode. On the other hand, the surface current on the ground plane at 1800 and 2200 MHz are relatively weaker because they are the 0.5λ and 1.0λ modes [1]. Furthermore, the currents on the ground plane at 2200 MHz is smaller than that at 1800 MHz because that the 1.0λ mode at 2200 MHz is known as a balanced mode. Figure 5(b) shows the vector surface currents on the loop strip. The current flows along the loop strip in the same direction for the 0.25λ mode (925 MHz). For the 0.5λ mode (1800 MHz), there are one current null along the loop strip, whereas there are two current nulls at the loop strip for the 1.0λ mode (2200 MHz). By considering the matching circuit as part of the complete current flow in the proposed antenna, the equivalent surface currents for the 0.5λ and 1.0λ modes are also shown in Figure 5(c) for comparison.

Effects of the gap widths t and d in the folded loop strip are also studied. The simulated results of the return loss for the width t varied from 0.5 to 3.5 mm are presented in Figure 6. Other dimensions are the same as studied in Figure 2. It is seen that the 0.5λ mode is almost not affected by the width t . Conversely, large variations in the 0.25λ and 1.0λ modes are seen. When a larger value of t is selected, the 0.25λ mode is shifted to lower frequencies, whereas the 1.0λ mode is shifted to higher frequencies. However, when t is larger than 1.5 mm, the bandwidth of the 0.25λ

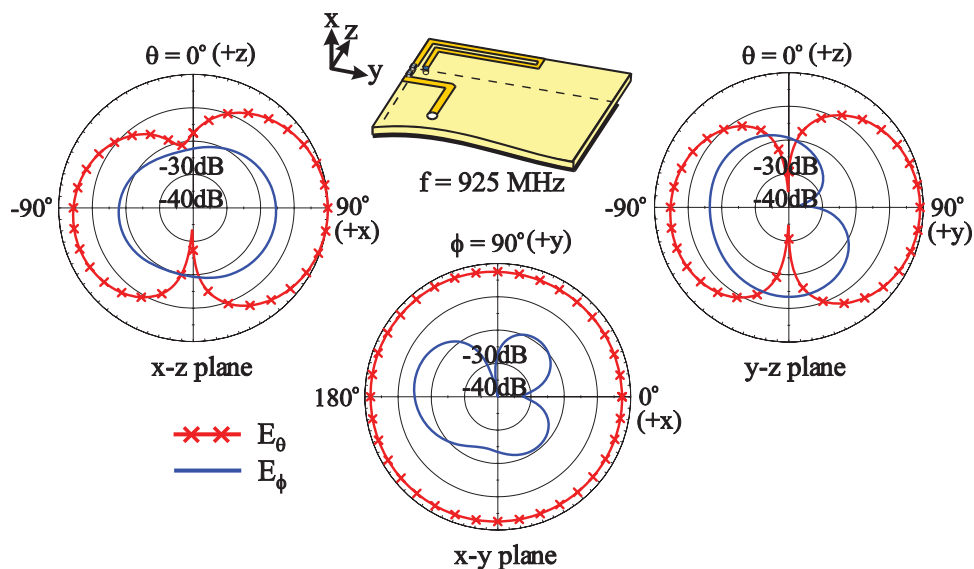


Figure 10 Measured radiation patterns at 925 MHz for the antenna studied in Figure 2. [Color figure can be viewed in the online issue, which is available at www.interscience.wiley.com]

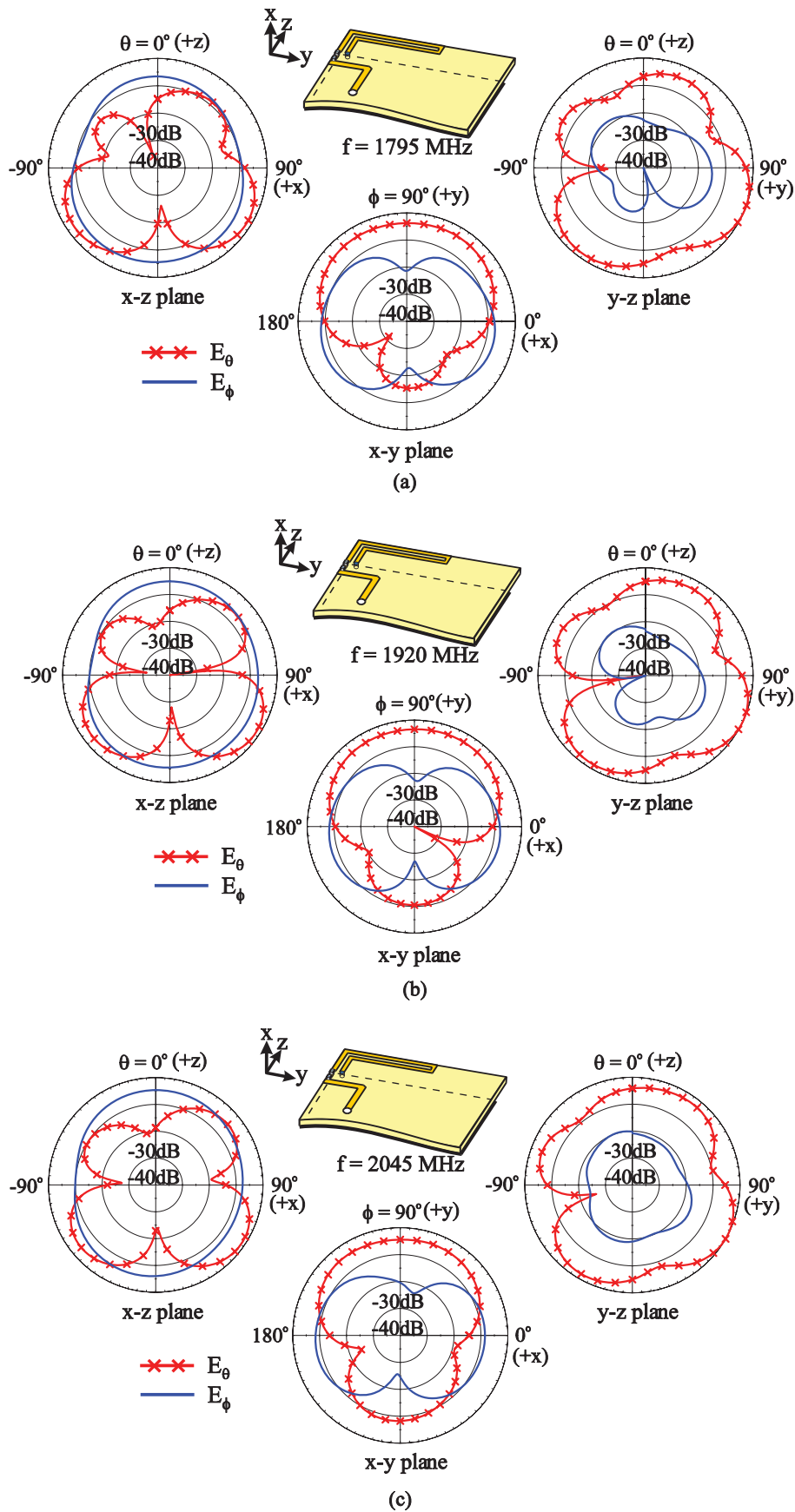


Figure 11 Measured radiation patterns at (a) 1795 MHz, (b) 1920 MHz, and (c) 2045 MHz for the antenna studied in Figure 2. [Color figure can be viewed in the online issue, which is available at www.interscience.wiley.com]

mode becomes smaller than that required for GSM operation. Hence, in this study, the width t is selected to be 1.5 mm for the antenna to generate a wide lower band for GSM operation; it can also lead to good impedance matching for the antenna's upper band formed by the 0.5λ and 1.0λ modes.

Effects of the gap width d are analyzed in Figure 7, in which the simulated return-loss results for d varied from 1 to 4 mm are presented. There is almost no effect on the 0.25λ mode. On the other hand, the resonant frequencies for the 0.5λ and 1.0λ modes are both shifted to higher frequencies when the width d increases. By selecting the width d to be 1 mm, the obtained upper band is suitable for DCS/PCS/UMTS operation. From the effects of t and d seen in Figures 6 and 7, we can first adjust the width t to obtain the desired lower band at about 900 MHz for GSM operation, and then tune the width d to obtain the desired upper band centered at about 2000 MHz for DCS/PCS/UMTS operation.

Effects of varying the capacitance and inductance in the matching circuit are analyzed in Figures 8 and 9. Simulated return-loss results for the capacitance C varied from 0.35 to 0.68 pF are presented in Figure 8. There is almost no effect on the 1.0λ mode. However, the resonant frequencies for the 0.25λ and 0.5λ modes are both shifted to lower frequencies when C increases. Further note that the impedance matching for the 0.25λ mode becomes poor when C is larger than 0.47 pF. By selecting C to be 0.47 pF, the obtained bandwidth for the 0.25λ mode is wide enough for GSM operation and the impedance matching over the upper band formed by the 0.5λ and 1.0λ modes are also better than 3:1 VSWR.

Figure 9 shows the simulated return-loss results for the inductance L varied from 11 to 15 nH. Small effects on the 0.25λ mode are seen as L varies. On the other hand, variations in L show large effects on the impedance matching of the 0.5λ and 1.0λ modes. This is an expected result because L in the matching circuit is mainly for the impedance matching compensation for frequencies over the antenna's upper band (also discussed in Fig. 4).

Figure 10 plots the measured radiation pattern at 925 MHz. Monopole-like radiation patterns at 925 MHz are seen, and omnidirectional radiation in the azimuthal plane (x - y plane) is generally observed. Figure 11 shows the measured radiation patterns at 1795, 1920, and 2045 MHz (center frequencies of the DCS, PCS, and UMTS bands, respectively). For the radiation patterns over the upper band, more variations and nulls in the patterns are seen. In the azimuthal plane (x - y plane), the radiation pattern in the $+y$ direction is larger than that in the $-y$ direction. This is mainly because the printed loop antenna is not symmetric to the central line of the system circuit board. Figure 12 presents the measured antenna gain and radiation efficiency. For frequencies over the GSM band, the antenna gain is about -0.7 to 0.4 dBi, whereas that for the DCS/PCS/UMTS bands ranges from about 0.8 to 3.1 dBi. The radiation efficiency is about 54–67% over the GSM band, whereas that over the DCS/PCS/UMTS band is about 55–85%.

4. CONCLUSION

A folded printed loop antenna with small length (62 mm) and occupied area (<100 mm²) and capable of GSM/DCS/PCS/UMTS operation in the mobile phone has been proposed. The loop antenna can operate at its 0.25λ mode as the lower band for covering GSM operation, and its 0.5λ and 1.0λ modes can also be generated to form the upper band for covering DCS/PCS/UMTS operation. The successful excitation of the three resonant modes is obtained by incorporating a simple series LC matching circuit. With proper selection of the series capacitor and inductor (0.47 pF and 13 nH here) in the matching circuit, the large inductive reactance of the 0.25λ mode of the loop antenna can be compensated, and good

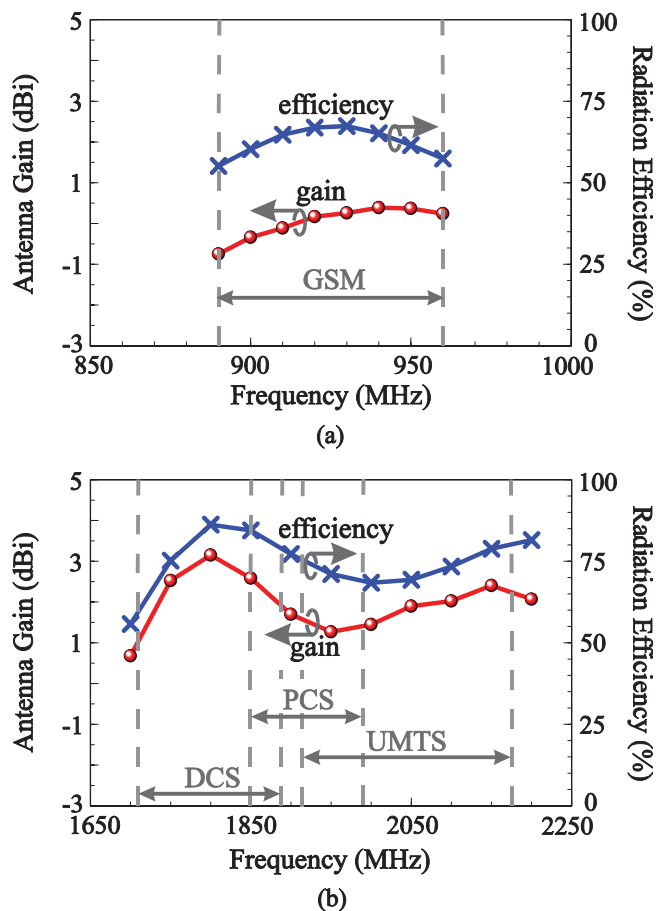


Figure 12 Measured antenna gain and radiation efficiency for the antenna studied in Figure 2. (a) The GSM band. (b) The DCS/PCS/UMTS band. [Color figure can be viewed in the online issue, which is available at www.interscience.wiley.com]

impedance matching over the 0.5λ and 1.0λ modes can also be achieved. A simple design rule for selecting the series capacitor and inductor has been provided in the paper. Good radiation characteristics for frequencies over the operating bands have also been obtained.

REFERENCES

1. Y.W. Chi and K.L. Wong, Internal compact dual-band printed loop antenna for mobile phone application, *IEEE Trans Antennas Propag* 55 (2007), 1457–1462.
2. W.Y. Li and K.L. Wong, Internal printed loop-type mobile phone antenna for penta-band operation, *Microwave Opt Technol Lett* 49 (2007), 2595–2599.
3. E. Lee, P.S. Hall, and P. Gardner, Dual band folded monopole/loop antenna for terrestrial communication system, *Electron Lett* 36 (2000), 1990–1991.
4. W.Y. Li and K.L. Wong, Surface-mount loop antenna for AMPS/GSM/DCS/PCS operation in the PDA phone, *Microwave Opt Technol Lett* 49 (2007), 2250–2254.
5. B.K. Yu, B. Jung, H.J. Lee, F.J. Harackiewicz, and B. Lee, A folded and bent internal loop antenna for GSM/DCS/PCS operation of mobile handset applications, *Microwave Opt Technol Lett* 48 (2006), 463–467.
6. B. Jung, H. Rhyu, Y.J. Lee, F.J. Harackiewicz, M.J. Park, and B. Lee, Internal folded loop antenna with tuning notches for GSM/GPS/DCS/PCS mobile handset applications, *Microwave Opt Technol Lett* 48 (2006), 1501–1504.
7. C.I. Lin and K.L. Wong, Internal meandered loop antenna for GSM/

- DCS/PCS multiband operation in a mobile phone with the user's hand, *Microwave Opt Technol Lett* 49 (2007), 759–765.
8. K.L. Wong, *Planar antennas for wireless communications*, Wiley, New York, 2003.
 9. J. Ollikainen, O. Kivekas, C. Ichein, and P. Vainikainen, Internal multiband handset antenna realized with an integrated matching circuit, *Proc 12th Int Conf Antennas Propag* 2 (2003), 629–632.
 10. J. Villanen, C. Ichein, and P. Vainikainen, A coupling element-based quad-band antenna element structure for mobile terminals, *Microwave Opt Technol Lett* 49 (2007), 1277–1282.
 11. M. Tzortzakakis and R.J. Langley, Quad-band internal mobile phone antenna, *IEEE Trans Antennas Propag* 55 (2007), 2097–2103.
 12. T. Ranta, Dual-resonant antenna, U.S. Patent No. 7,242,364, 2007.
 13. T. Oshiyama, H. Mizuno, and Y. Suzuki, Multi-band antenna, U.S. Patent Publication No. US 2007/0249313, 2007.
 14. C.H. Wu and K.L. Wong, Internal shorted planar monopole antenna embedded with a resonant spiral slot for penta-band mobile phone application, *Microwave Opt Technol Lett* 50 (2008), 529–536.
 15. C.H. Chang, K.L. Wong, and J.S. Row, Multiband surface-mount chip antenna integrated with the speaker in the mobile phone, *Microwave Opt Technol Lett* 50 (2008), 1126–1132.
 16. S.L. Chien, F.R. Hsiao, Y.C. Lin, and K.L. Wong, Planar inverted-F antenna with a hollow shorting cylinder for mobile phone with an embedded camera, *Microwave Opt Technol Lett* 41 (2004), 418–419.
 17. Ansoft Corporation, Available at <http://www.ansoft.com/products/hf/hfss/>, Ansoft Corporation HFSS.

© 2008 Wiley Periodicals, Inc.

SYSTEMATIC DESIGN AND REALIZATION OF THE OPTICAL FEEDFORWARD TRANSMITTER BASED ON MICROWAVE CIRCUIT MODELING

Yon-Tae Moon,¹ Jun Woo Jang,¹ Tae-Kyeong Lee,¹ Do-Gyun Kim,¹ Ho-Hyun Park,¹ Tae-Gu Kang,² Sang-Kook Han,³ and Young-Wan Choi¹

¹ School of Electrical and Electronics Engineering, Chung-Ang University, 221 Heuksuk-Dong, Dongjak-ku, Seoul 156-756, Korea; Corresponding author: ychoi@cau.ac.kr

² School of Electrical and Electronic Engineering and Computer Science, Kyungpook National University, Sangyeok-dong, Buk-gu, Daegu 702-701, Korea

³ Department of Electrical and Electronic Engineering, Yonsei University, Shinchon-Dong, Seodaemun-Ku, Seoul 120-749, Korea

Received 15 May 2008

ABSTRACT: We have systematically designed and realized the optical feedforward transmitter using microwave circuit model of distributed-feedback laser diode (DFB LD) based on rate equations. Through the system-level simulation for the optical feedforward method, the nonlinearity of DFB-LD is analyzed, and the optimized characteristics of the RF components in the system are confirmed by using a microwave simulator. The experimental and simulated results show the reduced distortion products and enhanced spurious-free dynamic ranges are in good agreement at 2.4 GHz. These results are analyzed as the evaluation parameters for the miniaturization and optimization of the feedforward compensation method in radio-over-fiber systems. © 2008 Wiley Periodicals, Inc. *Microwave Opt Technol Lett* 51: 192–195, 2009; Published online in Wiley InterScience (www.interscience.wiley.com). DOI 10.1002/mop.24007

Key words: linearization; intermodulation distortion products; feedforward compensation method; distributed-feedback laser diode

1. INTRODUCTION

Radio-over-Fiber (RoF) attracts the attention of radio access network infrastructure, because it can give user the higher bit rates and broad transmission with multimedia services [1]. RoF is a promising technique for the deployment of highly flexible and cost-effective radio access system [2]. In these systems, radio frequency signals are modulated onto an optical carrier at a central station, and then distributed to remote base stations through optical channel. The base stations then transmit RF signals to mobile stations with microwave antennas over cell areas. Within these wire/wireless networks, main issues are for reduction in cost, size, and total system complexity. In the typical RoF systems, the directly modulated distributed-feedback laser diode (DFB-LD), as the key component of RoF link, is preferred to reduce the system cost. However, the DFB-LDs have nonlinear characteristics, which degrade the overall system performance [3]. The limitation can be overcome by linearization techniques. A number of linearization methods have been reported to reduce nonlinear distortion products of a direct-modulated LD [3–6]. The optical feed-forward technique provides better linearity and wider bandwidth than the other techniques as shown in Figure 1. However, it has disadvantages such as higher cost and complexity of the total system. The reported optical feed-forward transmitter was demonstrated by using hybrid-typed RF and optical components; therefore, the transmitter volume was bulky [5, 6]. Generally, the compact optical transmitter has many merits as system construction cost and maintenance in the in-building RoF system. For the realization of the compact system, analysis of LD and confirmation for RF circuit performance to precisely match the signal amplitude and phase in each path of the optical feedforward system should be resolved. As using extracting values of the rate equation parameters in a commercial microwave simulator, the system-level simulation confirms a predesign and also accurately predicts the important characteristics of the feed-forward scheme.

In this article, the DFB-LD model is implemented by symbolically defined devices (SDDs) in the Hewlett-Packard Advanced Design System (HP-ADS). The laser model and RF component circuit models enable the microwave simulator to analyze the nonlinear characteristics of laser diodes in the optical feed-forward method. The simulation results are compared with experimental results to verify the system-level simulation performance.

2. CIRCUIT MODELING OF DITRIBUTED-FEEDBACK LASER DIODE

The rate equations of laser diode describe relation of the injection current I , the electron density N , and the photon density S , hence it was often used to analyze the LD behavioral performance [7]. Rate equation analysis can also predict LD dynamic characteristics, such as small signal, thermal effect, noise, and large signal [8, 9]. We establish the suitable circuit model of DFB-LD based on rate equations as follows: [10]

$$\frac{dN}{dt} = \frac{I}{qV_{\text{act}}} - g(N - N_0)(1 - \epsilon S)S - \frac{N}{\tau_n}, \quad (1)$$

$$\frac{dS}{dt} = \Gamma g(N - N_0)(1 - \epsilon S)S - \frac{S}{\tau_s} - \Gamma \beta \frac{N}{\tau_n}, \quad (2)$$

where V_{act} is the active region volume, g is the gain coefficient, N_0 is the optical transparency density, ϵ is the phenomenological gain compression factor, τ_n and τ_s is the electron and photon lifetime, Γ is the optical confinement factor, β is the spontaneous emission coupling factor, and q is the electron charge.